Stochastic asymmetry properties of 3D gauss-lagrange ocean waves with directional spreading

Stochastic asymmetry properties of 3D Gauss-Lagrange ocean waves with directional spreading

Georg Lindgren
Mathematical Statistics, Lund University, Sweden
Finn Lindgren
Department of Mathematical Sciences, NTNU, Trondheim, Norway

Abstract

In the stochastic Lagrange model for ocean waves the vertical and horizontal location of surface water particles are modeled as correlated Gaussian processes. In this paper we investigate the statistical properties of wave characteristics related to wave asymmetry in the 3D Lagrange model. We present a modification of the original Lagrange model that can produce front-back asymmetry both of the space waves, i.e. observation of the sea surface at a fixed time, and of the time waves, observed at a fixed measuring station. The results, which are based on a multivariate form of Rice's formula for the expected number of level crossings, are given in the form of the cumulative distribution functions for the slopes observed either by asynchronous sampling in space, or at synchronous sampling at upcrossings and downcrossings, respectively, of a specified fixed level. The theory is illustrated in a numerical section, showing how the degree of wave asymmetry depends on the directional spectral spreading and on the mean wave direction. It is seen that the asymmetry is more accentuated for high waves, a fact that may be of importance in safety analysis of capsizing risk.

Keywords: Crossing theory, directional spreading, front-back asymmetry, Gaussian process, Palm distribution, Rice formula, slope asymmetry, wave steepness.
AMS 2000 Subject Classification: Primary 60G15. Secondary 60G70, 74J05, 74J30, 76B15, 86A05

1 Introduction

The statistical distribution of ocean wave slopes is an important parameter in many types of oceanographic applications, which depend on a reflected radar signal. Reliable models for the slope distributions are needed for correct calibration of algorithms used in remote sensing of ocean wind and wave fields, ocean temperature, and many other variables. The distribution is also important for the understanding of physical wave mechanisms and in the safety analysis of marine vessels. A special topic in the study of wave slope distributions is the question of front-back asymmetry, namely the fact that for wind-driven waves, the leeward wave front is in general steeper than the wave back.

The statistical distribution of wave slopes in general, and front-back asymmetry in particular, has been the subject of several systematic empirical studies, beginning with Cox and Munk [6], [7], reanalyzed by Plant [22]. An example of an empirically fitted slope distribution by Cox and Munk, together with a theoretical slope distribution in a first-order Lagrange model, can be seen in Figure 1. Of special interest for the model developed in this paper are the work by Longuet-Higgins [19], Bailey et al. [4], Ebuchi and Kizu [8], and Walsh et al. [27]; see also [12, Sect. 6.4.3].

Longuet-Higgins discusses several possible mechanisms for the generation of front-back asymmetry, and gives supporting evidence for the influence of the horizontal wind. Bailey et al. separate young wind-driven asymmetric waves and old waves with less asymmetry. Ebuchi and Kizu fail to observe any front-back asymmetry at all in the wind direction, using sun glitter images from a meteorological satellite, and attribute this to inhomogeneous sea states in the observed areas. Walsh et al. discuss further the wind related asymmetries for long and short waves, based on airborne radar altimetry measurements. For more on the empirical background and a historical overview of measurement campaigns, the reader is referred to the cited papers, and also to [9] and [15],

Most theoretical studies of front-back wave asymmetry are based on non-linear interaction models or on non-linear differential equation models, and it is difficult to perform a full theoretical analysis of their statistical properties. The first-order Lagrange model is a linear model, giving room for explicit statistical analysis. At the same time, it is flexible enough to reproduce the statistical features, empirically observed in real ocean waves.

The stochastic Lagrange wave model treated in this paper is a realistic alternative to the Gaussian linear model. Stochastic Lagrange models were introduced and studied by Gjøsund [10], Socquet-Juglard et al. [24],

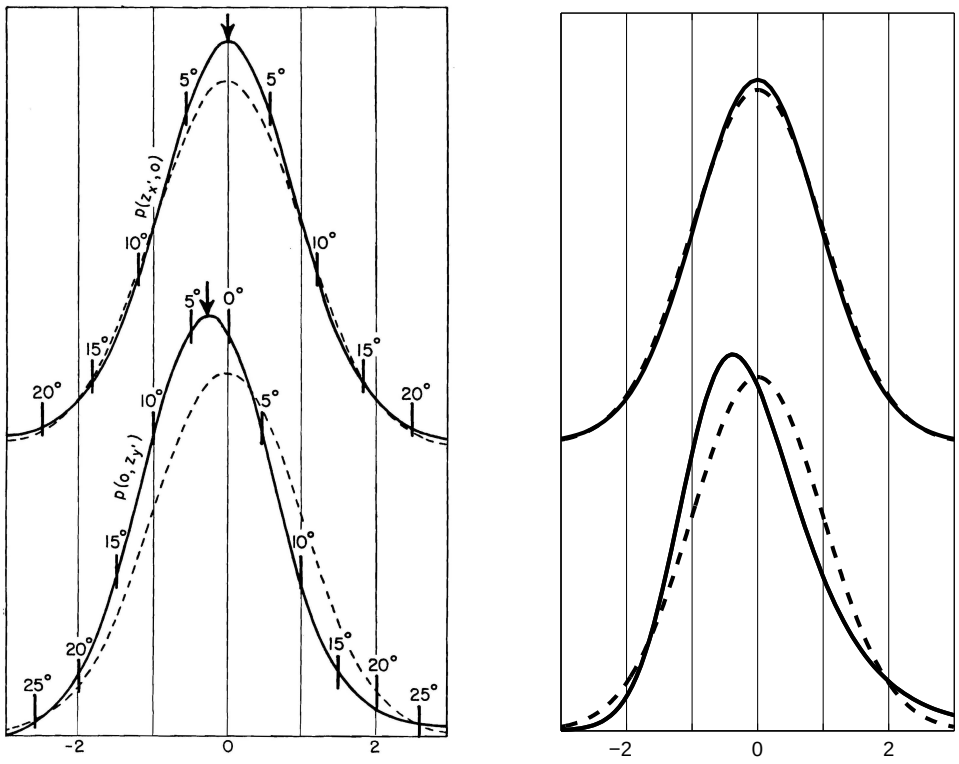

Figure 1: *Left:* Illustration from Cox and Munk [6, Fig. 8] of approximate normalized slope density functions in along-wind (lower curves) and cross-wind (upper curves) direction, estimated from sun glitter over an area, together with standard normal densities (dashed). *Right:* Slope densities calculated in the 3D Lagrange model with Pierson-Moskowitz orbital spectrum with considerable directional spreading. (For definition of orbital spectrum, see Section 2.1.1.) The density has been modified to resemble the Cox and Munk figure, with wave front slopes being positive; for details, see Sections 3.2 and 5.2.

and Fouques et al. [9], who showed that Monte Carlo simulated stochastic Lagrange models can produce realistic crest-trough asymmetry as well as front-back asymmetry, the latter for higher order Lagrange models. Theoretical studies of their stochastic properties have recently been made by Lindgren [14], Aberg [1], Aberg and Lindgren [2], Lindgren and Aberg [17], and Lindgren [15, 16]. All these work deal with uni-directional waves observed in time at a fixed location or along a line with a fixed direction in space, equivalent to 2D waves with one space parameter together with the time parameter. They describe their space and time properties, and it is noticeable that the time properties require a more complicated stochastic analysis than the space properties.

Two very recent models also appear to be able to model stochastic asymmetry in a realistic and practically useful way. The first one is a stochastic partial differential equation (SPDE), introduced by Bolin and Lindgren [5], see also [18]. The second model is a moving average model driven by a generalized Laplace processes; see Podgórski and Wegener [23].

In this paper, we generalize the study to 3D Lagrange waves with directional spreading, observed as space waves at a fixed time, observed over an area or along a section of the sea surface, or as time waves, at a fixed observation point. We derive the statistical distributions of slopes observed with asynchronous area sampling, and observed at up- and downcrossings of a fixed level, and illustrate by examples how the properties of the space wave slopes vary with the degree of directional spreading in the energy spectrum and with the mean wave direction.

The first-order 3D stochastic Lagrange model is presented in Section 2. Sections 3 and 4 contain the definitions of slopes in space and time waves, respectively, and give the main results on the exact statistical distribution of asynchronous slopes and of slopes at up- and downcrossings. Section 5, finally, illustrates the theory in some numerical examples, showing how the degree of directional spreading and main wave direction influence the stochastic front-back asymmetry of the space waves.

2 The 3D stochastic Lagrange wave model

2.1 The Gaussian wave field

2.1.1 Definition and basic properties

To define the 3D Lagrange model, we first introduce a Gaussian time-varying random field $W(t, \boldsymbol{s})$ with time parameter t and space parameter $\boldsymbol{s} = (u, v)$. In the Gaussian linear wave model, $W(t, \boldsymbol{s})$ would be the surface elevation

relative to the still water level at time t at location $\boldsymbol{s}$. In the Lagrange model, we will use W to denote the height of individual water particles, as will be described in Section 2.2.

The Gaussian process $W(t, \boldsymbol{s})$ is assumed to have mean zero and to be stationary in time and homogeneous in space. This means that it can be expressed as a stochastic integral over wavenumber $\boldsymbol{\kappa} = (\kappa_x, \kappa_y) \in \mathbb{R}^2$, or, alternatively, over wave angular frequency $\omega > 0$ and wave direction $\theta \in (-\pi, \pi]$. Wave number and frequency/direction are related via the dispersion relation, which also includes water depth h; see [13, Ch. 4]. With $\kappa = \sqrt{\kappa_x^2 + \kappa_y^2}$, the dispersion relation is

$$\omega = \omega(\boldsymbol{\kappa}) = \sqrt{g\kappa \tanh \kappa h}, \tag{1}$$

$$\theta = \arctan_2(\kappa_y, \kappa_x), \tag{2}$$

with the inverse

$$\boldsymbol{\kappa} = \boldsymbol{\kappa}(\omega, \theta) = (\kappa_x, \kappa_y), \quad \kappa_x = \kappa \cos\theta, \quad \kappa_y = \kappa \sin\theta.$$

Here g denotes the earth gravitation constant. For infinite water depth, relation (1) reduces to $\omega = \sqrt{g\kappa}$. In (2), $\arctan_2$ is the four quadrant inverse tangent function.

We denote by τ and $\boldsymbol{\sigma} = (\sigma_x, \sigma_y)$ a time difference and a space difference, respectively. The covariance function of the field in space-time is then, with $\boldsymbol{\kappa\sigma} = \kappa_x\sigma_x + \kappa_y\sigma_y$,

$$\begin{aligned} r^{ww}(\tau, \boldsymbol{\sigma}) &= \mathsf{Cov}(W(t, \boldsymbol{s}), W(t+\tau, \boldsymbol{s}+\boldsymbol{\sigma})) \\ &= \int_{\omega=0}^{\infty} \int_{\theta=-\pi}^{\pi} \cos(\boldsymbol{\kappa\sigma} - \omega\tau)\, S(\omega, \theta)\, \mathrm{d}\omega\, \mathrm{d}\theta, \end{aligned} \tag{3}$$

where $S(\omega, \theta)$, for $\omega > 0$, $-\pi < \theta \leq \pi$, is the directional spectrum of the field. In the entire paper, we assume all processes to be ergodic, so the spectrum is continuous and all covariances vanish at infinity. Following Fouques et al. [9], we call the spectral density $S(\omega, \theta)$ the *orbital spectrum*, indicating that it refers to the orbital motions of water particles in the Lagrange model; see also Remark 4.

2.1.2 A complex representation

The real form (3) of the spectral representation of the covariance function is the form used in most applications. It turns out, that the definition of the Lagrange waves becomes mathematically simpler with a complex formulation. We therefore express the *real* Gaussian process as a stochastic

integral of a *complex* spectral process, $\zeta(\boldsymbol{\kappa}, \omega)$. To achieve this, we extend the wave number-frequency space from $(\boldsymbol{\kappa}, \omega) \in \mathbb{R}^2 \times \mathbb{R}^+$ to $\mathbb{R}^2 \times \mathbb{R}$ by allowing also $(\boldsymbol{\kappa}, \omega) \in \mathbb{R}^2 \times \mathbb{R}^-$, identifying a wave characterized by a certain set $(\kappa_x, \kappa_y; \omega, \theta)$ with a wave with characteristics $(-\kappa_x, -\kappa_y; -\omega, \theta + \pi \bmod 2\pi)$, reflecting $(\kappa_x, \kappa_y, \omega)$ in the origin.

With $S(\omega, \theta), (\omega, \theta) \in \mathbb{R}^+ \times (-\pi, \pi]$, the directional frequency spectrum of $W(t, \boldsymbol{s})$, we write

$$\widetilde{S}(\omega, \theta) = \begin{cases} \frac{1}{2}\, S(\omega, \theta), & \text{if } \omega > 0, \\ \frac{1}{2}\, S(-\omega, \theta + \pi \bmod 2\pi), & \text{if } \omega < 0, \end{cases}$$

for the spectrum on the extended space $\mathbb{R} \times (-\pi, \pi]$.

If one reflects $(\kappa_x, \kappa_y, \omega)$ in the origin one can define the spectral representation in a symmetric complex form. Writing

$$D = \left\{ (\boldsymbol{\kappa}, \omega) \in \mathbb{R}^3; \omega = \pm\sqrt{g\kappa \tanh \kappa h} \right\},$$

for the dispersion surface, one has, with a small abuse of notation, and with $\boldsymbol{\kappa}\boldsymbol{s} = \kappa_x u + \kappa_y v$,

$$\begin{aligned} W(t, \boldsymbol{s}) &= \int_{(\boldsymbol{\kappa}, \omega) \in D} e^{i(\boldsymbol{\kappa}\boldsymbol{s} - \omega t)}\, \mathrm{d}\zeta^K(\boldsymbol{\kappa}, \omega) \\ &= \int_{\omega=-\infty}^{\infty} \int_{\theta=-\pi}^{\pi} e^{i(\boldsymbol{\kappa}\boldsymbol{s} - \omega t)}\, \mathrm{d}\zeta(\omega, \theta). \end{aligned} \tag{4}$$

Here $\zeta^K(\boldsymbol{\kappa}, \omega)$ is a Gaussian complex spectral process with mean 0 such that

$$\mathrm{d}\zeta^K(-\boldsymbol{\kappa}, -\omega) = \overline{\mathrm{d}\zeta^K(\boldsymbol{\kappa}, \omega)},$$

($\overline{z}$ denoting complex conjugate of z), and $\zeta(\omega, \theta)$ the corresponding spectral process in the (ω, θ)-plane process with

$$\mathrm{d}\zeta(-\omega, \theta) = \overline{\mathrm{d}\zeta(\omega, \theta + \pi \bmod 2\pi)}.$$

Furthermore,

$$E\left(\mathrm{d}\zeta(\omega, \theta) \cdot \overline{\mathrm{d}\zeta(\omega', \theta')}\right) = \begin{cases} 0, & \text{if } \omega \neq \omega' \text{ or } \theta \neq \theta', \\ \widetilde{S}(\omega, \theta)\, \mathrm{d}\omega\, \mathrm{d}\theta, & \text{if } \omega = \omega', \theta = \theta'. \end{cases} \tag{5}$$

2.2 The first-order Lagrange wave model

2.2.1 The free Lagrange model

The integral (4) defines the waves as a continuous version of a sum of independent cosine waves, with different directions and frequencies, and in the

Gaussian model it gives the elevation of the free water level relative the still water level at location $\boldsymbol{s} = (x, y)$ at time t. The (first-order) stochastic Lagrange model is built in a similar way, but instead of letting $W(t, \boldsymbol{s})$ be the relative height of the free water level at the fixed point (x, y), as in the Gaussian model, we let it describe the height at a varying point $(X(t, \boldsymbol{s}), Y(t, \boldsymbol{s}))$, which performs a random shift around $\boldsymbol{s} = (u, v)$, the *reference point*. The physical interpretation of the model is that $W(t, \boldsymbol{s}), X(t, \boldsymbol{s}), Y(t, \boldsymbol{s})$ are the vertical and horizontal coordinates of an individual water particle on the surface. The original horizontal location of the particle is $\boldsymbol{s} = (u, v)$.

From the linearized hydrodynamic equations, (see Fouques et al. [9]), the random shift process, $(X(t, \boldsymbol{s}), Y(t, \boldsymbol{s}))$, is defined by linear filtrations of $W(t, \boldsymbol{s})$. To this end, introduce the complex transfer function vector (with subscript M denoting Miche waves; [20]),

$$\boldsymbol{H}_M(\theta, \kappa) = \begin{pmatrix} h_x(\theta, \kappa) \\ h_y(\theta, \kappa) \end{pmatrix} = i \, \frac{\cosh \kappa h}{\sinh \kappa h} \begin{pmatrix} \cos\theta \\ \sin\theta \end{pmatrix}, \ \theta \in (-\pi, \pi], \tag{6}$$

and define, integrating over $(\omega, \theta) \in \mathbb{R} \times (-\pi, \pi]$,

$$\boldsymbol{\Sigma}(t, \boldsymbol{s}) = \begin{pmatrix} X_M(t, \boldsymbol{s}) \\ Y_M(t, \boldsymbol{s}) \end{pmatrix} = \boldsymbol{s} + \int_\omega \int_\theta \boldsymbol{H}_M(\theta, \|\boldsymbol{\kappa}\|) \, e^{i(\boldsymbol{\kappa}\boldsymbol{s} - \omega t)} \, \mathrm{d}\zeta(\omega, \theta). \tag{7}$$

Remark 1. *Expressions for the auto- and cross-covariance functions between the vertical and horizontal processes are given in Appendix A. In the sequel we use upper index in a covariance function to indicate the processes to be correlated, e.g. r^{ww} is the auto-covariance function for W, and we use lower index to indicate that the covariance function is between derivative processes. For example, r^{wx}_{tu} is the cross-covariance function between $\partial W/\partial t$ and $\partial X/\partial u$, and $r^{wy}_{t(uv)}$ is the covariance function between $\partial W/\partial t$ and $\partial^2 Y/\partial u \partial v$.*

2.2.2 The linked Lagrange model

The free Lagrange model (7) will generate front-back statistically symmetric waves. To obtain realistic asymmetries it is necessary to introduce a more general transfer function than the purely imaginary Miche function $\boldsymbol{H}_M(\theta, \kappa)$ in Eqn. (6), and consider a transfer function,

$$\boldsymbol{H}(\theta, \kappa) = \begin{pmatrix} h_x(\theta, \kappa) \\ h_y(\theta, \kappa) \end{pmatrix} = \begin{pmatrix} \rho_x(\theta, \kappa) \, e^{i\psi_x(\theta, \kappa)} \\ \rho_y(\theta, \kappa) \, e^{i\psi_y(\theta, \kappa)} \end{pmatrix}. \tag{8}$$

The general expression for the horizontal displacement will then be

$$\begin{aligned}\boldsymbol{\Sigma}(t,\boldsymbol{s}) &= \begin{pmatrix} X(t,\boldsymbol{s}) \\ Y(t,\boldsymbol{s}) \end{pmatrix} \\ &= \boldsymbol{s} + \int_\omega \int_\theta \begin{pmatrix} e^{i(\kappa_x u + \kappa_y v - \omega t + \psi_x(\theta,\kappa))} \rho_x(\theta,\kappa) \\ e^{i(\kappa_x u + \kappa_y v - \omega t + \psi_y(\theta,\kappa))} \rho_y(\theta,\kappa) \end{pmatrix} \mathrm{d}\zeta(\omega,\theta).\end{aligned}$$

It is seen that the free model introduces a constant phase shift of $\psi_x = \psi_y = \pi/2 = 90^o$ between the vertical and horizontal processes, while the linked model requires a more general and frequency dependent phase shift.

In the examples we will use a complex transfer function that, besides the imaginary component $H_M(\theta,\kappa)$, contains a real term, whose form remains to be determined. Working with the 2D model, Lindgren and Aberg [17] argued for a wind-driven dependence between the vertical field and the horizontal acceleration of the form

$$\frac{\partial^2}{\partial t^2} X(t,\boldsymbol{s}) = \frac{\partial^2}{\partial t^2} X_M(t,\boldsymbol{s}) - \alpha W(t,\boldsymbol{s}), \tag{9}$$

where the *linkage parameter* α determines the degree of front-back asymmetry. The motivation for the relation was that it represents the effect of a wind blowing in the x-direction, $\theta = 0$. The corresponding transfer function is $H_M(\kappa) + \alpha/\omega^2$. Figure 2 gives an illustration of how the elliptic particle orbits are tilted by the frequency dependent phase shift. In the figure, $\alpha = 0.3$ and the water depth $h = 32\,\mathrm{m}$.

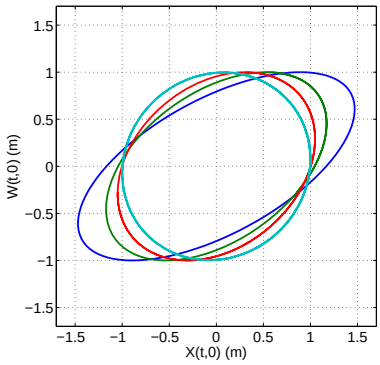

Figure 2: Frequency dependent particle orbits in model (9) with $\alpha = 0.3$, $h = 32\,\mathrm{m}$, and waves with frequencies, $\omega = 0.58$ (most eccentric), 0.75, 1, 2 (least eccentric).

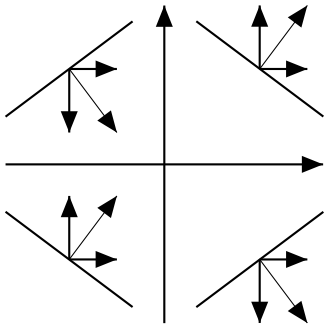

Figure 3: Forces, in model (10), from wind blowing in the x-direction, on waves with different orientations; see Remark 2.

For the 3D case, we have chosen to keep the term α/ω^2 but modify it according to wave direction θ. The following choice will be used in the examples in Section 5:

$$\boldsymbol{H}(\theta,\kappa) = \frac{\alpha}{\omega^2}\cdot\begin{pmatrix}\cos^2(\theta)\,|\cos(\theta)|\\ \cos^2(\theta)\sin(\theta)\,\mathrm{sign}(\cos\theta)\end{pmatrix} + i\frac{\cosh\kappa h}{\sinh\kappa h}\cdot\begin{pmatrix}\cos\theta\\ \sin\theta\end{pmatrix}. \quad (10)$$

Remark 2. *This specific direction dependence is chosen so it should resemble the effect of a constant wind blowing in the x-direction, $\theta = 0$. As it turns out, the final results concerning the front-back asymmetry are not very sensitive to the exact form of the real part of the transfer function, as long as it treats the four quadrants in a logical way. Figure 3 illustrates how the wind in the x-direction affects wave fronts moving out from the origin in different directions. The horizontal component of the force vector (thick arrows) always point in the positive x-direction, while the vertical component point in the positive or negative y-direction, in agreement with the sign given in the real part of* (10)*. The* $\cos^2\theta$ *factor is the total force vector (thin arrows).*

Since the exact mechanism in the wind-wave interaction is very complicated, and no unique model seems to be established in the literature, we have chosen to illustrate the theory on the model (10)*, even if it is chosen a bit ad hoc.*

It should be noted, however, that the model (10) *is not of full rank, but will produce linearly dependent space derivatives: $\partial X/\partial u = \partial Y/\partial v$. This will not affect the slope distributions, studied in this paper.*

2.2.3 Space and time waves and their derivatives

Definition 1. The first-order 3D Lagrange model for ocean waves is the tri-variate Gaussian process $(\boldsymbol{\Sigma}(t,\boldsymbol{s}), W(t,\boldsymbol{s}))$, $t\in\mathbb{R}$, $\boldsymbol{s}\in\mathbb{R}^2$. The time dependent Lagrange wave field can be implicitly expressed as

$$L(t,\boldsymbol{\Sigma}(t,\boldsymbol{s})) = W(t,\boldsymbol{s}). \quad (11)$$

Remark 3. *A complication in the model is that folding may occur, leading to multiple values of L in some areas, i.e. it can happen that $\boldsymbol{\Sigma}(t_0,\boldsymbol{s}_1) = \boldsymbol{\Sigma}(t_0,\boldsymbol{s}_2)$ with $\boldsymbol{s}_1\neq\boldsymbol{s}_2$, and $W(t_0,\boldsymbol{s}_1)\neq W(t_0,\boldsymbol{s}_2)$. However, for realistic parameter values and water depth, the probability of folding is negligible. The relation* (11) *defines the Lagrange field locally as a smooth differentiable time variable surface.*

By keeping either time or space coordinates fixed, $t = t_0$, and $(x,y) = (x_0,y_0)$, respectively, we obtain the two types of wave observations, recorded in empirical studies.

The space wave field is defined implicitly by the relation (11) for fixed $t = t_0$, or explicitly, if there is only one $\boldsymbol{s} = \boldsymbol{\Sigma}^{-1}(t_0, (x, y))$ satisfying $\boldsymbol{\Sigma}(t_0, \boldsymbol{s}) = (x, y)$, by

$$L(t_0, (x, y)) = W(t_0, \boldsymbol{\Sigma}^{-1}(t_0, (x, y))).$$

The time wave $L(t, (x_0, y_0))$ at a fixed location (x_0, y_0), is defined as the parametric curve

$$t \mapsto W(t, \boldsymbol{\Sigma}^{-1}(t, (x_0, y_0))),$$

provided $\boldsymbol{\Sigma}^{-1}(t, (x_0, y_0)) = \{\boldsymbol{s}; \boldsymbol{\Sigma}(t, \boldsymbol{s}) = (x_0, y_0)\}$ is uniquely defined at time t. Then, there is only one water particle located at position (x_0, y_0) at time t. Otherwise, the Lagrangian time wave takes multiple values.

Remark 4 (A remark about orbital and other spectra)**.** *When the first-order Lagrange model is used to describe real ocean waves, it is the spectral density, Ψ_1, say, of $L(t, x, y)$ that shall be compared to the spectral density estimated from wave observations.*

The orbital spectrum $S(\omega, \theta)$ is defined by (3) *as the Fourier transform of the covariance function of the vertical process W, and it satisfies* (5)*. Fouques et al. [9] present an expression for Ψ_1, and they state that $S(\omega, \theta)$ can be used as a good approximation for small values of the wave steepness. However, due to the non-uniqueness of the inverse space transformation, the precise meaning of their definition is not quite clear.*

Figure 4 shows examples of asymmetric 2D Lagrange space and time waves on extremely shallow water (to clearly show the asymmetry), and with $\alpha = 0.4$ in the linked model (10). The orbital spectrum is the unidirectional Pierson-Moskowitz (PM) spectrum described in Section 5.

The wave slopes in the two models can be expressed in terms of the partial derivatives, found by direct differentiation of (11):

$$\begin{pmatrix} W_u \\ W_v \end{pmatrix} = \begin{pmatrix} X_u & Y_u \\ X_v & Y_v \end{pmatrix} \begin{pmatrix} L_x \\ L_y \end{pmatrix}, \tag{12}$$

$$W_t = L_t + \begin{pmatrix} X_t & Y_t \end{pmatrix} \begin{pmatrix} L_x \\ L_y \end{pmatrix}, \tag{13}$$

where L_t, L_x, L_y denote the local derivatives, on the branch determined by the reference coordinates. When the inverse exists, we obtain the explicit

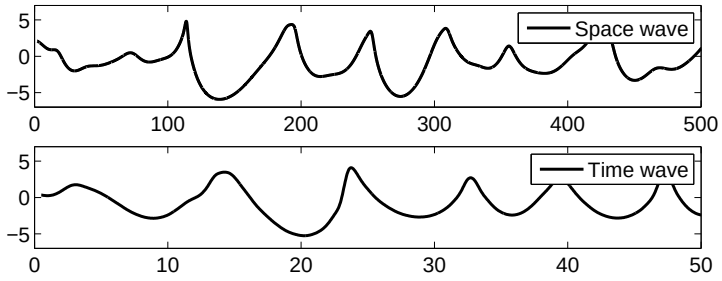

Figure 4: Exaggerated examples of asymmetric Lagrange space and time waves with Pierson-Moskowitz orbital spectrum; horizontal axis units are (m) and (s), respectively.

relations,

$$\begin{pmatrix} L_x \\ L_y \end{pmatrix} = \begin{pmatrix} X_u & Y_u \\ X_v & Y_v \end{pmatrix}^{-1} \begin{pmatrix} W_u \\ W_v \end{pmatrix}, \tag{14}$$

$$L_t = W_t - \begin{pmatrix} W_u & W_v \end{pmatrix} \begin{pmatrix} X_u & X_v \\ Y_u & Y_v \end{pmatrix}^{-1} \begin{pmatrix} X_t \\ Y_t \end{pmatrix}. \tag{15}$$

3 Slope distribution for 3D space waves

3.1 Definition of space wave and its slope

The Lagrange space wave is what is seen in a photo or radar image of the sea surface, like in the study by Cox and Munk [6], and in many subsequent studies. The statistical distribution of space wave characteristics, such as crest height, wave length, etc, are to be interpreted in a frequentistic way as what one can empirically observe from observations of an infinitely extended, statistically homogeneous, section of the ocean. Then, one has to define precisely how the observations are to be made – either by *asynchronous sampling* of the surface at a fixed grid in space, or by *synchronous sampling* at locations defined by some specified type of random event defined by the process to be measured, in our case, the presence of a level crossing.

We consider space waves observed at time $t_0 = 0$, and to simplify notation, we leave out the time parameter in the following analysis.

From (14), we obtain the derivative at location (x, y) expressed in terms

of the partial derivatives at the reference point $\boldsymbol{s} = \boldsymbol{\Sigma}^{-1}(x, y)$, e.g.

$$\begin{pmatrix} L_x(x,y) \\ L_y(x,y) \end{pmatrix} = \mathbf{L}'(x,y) = \begin{pmatrix} \frac{Y_v(\boldsymbol{s})W_u(\boldsymbol{s}) - Y_u(\boldsymbol{s})W_v(\boldsymbol{s})}{Y_v(\boldsymbol{s})X_u(\boldsymbol{s}) - Y_u(\boldsymbol{s})X_v(\boldsymbol{s})} \\ \frac{X_v(\boldsymbol{s})W_u(\boldsymbol{s}) - X_u(\boldsymbol{s})W_v(\boldsymbol{s})}{Y_v(\boldsymbol{s})X_u(\boldsymbol{s}) - Y_u(\boldsymbol{s})X_v(\boldsymbol{s})} \end{pmatrix}, \tag{16}$$

valid at each point on the space surface.

It will be convenient to introduce a notation $\widetilde{\mathbf{L}}(t, \boldsymbol{s}) = L(t, \boldsymbol{\Sigma}(t, \boldsymbol{s})) = W(t, \boldsymbol{s})$, and to distinguish between $\mathbf{L}(t, (x, y))$ and $\widetilde{\mathbf{L}}(t, \boldsymbol{s})$. With this notation

$$\widetilde{\mathbf{L}}'(\boldsymbol{s}) = \begin{pmatrix} \widetilde{L}_x(\boldsymbol{s}) \\ \widetilde{L}_y(\boldsymbol{s}) \end{pmatrix}$$

is the right hand side of (16), and it gives a unique definition of the space slope for each solution.

For a fixed pair $\boldsymbol{s} = (u, v)$, the slopes in (16) are just the ratios between quadratic forms in a six-variate normal distribution, and the distribution can be found by integrating the multivariate density. However, we seek the conditional slope distribution of the space wave, *conditioned* on the event $(X(\boldsymbol{s}), Y(\boldsymbol{s})) = (x_0, y_0)$, in the asynchronous case, and on the event that (x, y) is a crossing point in a specified direction, in the synchronous case.

We will now separate the analysis and deal first with asynchronous sampling, where $(x, y) = (x_0, y_0)$ is a fixed coordinate point, and then with synchronous sampling, where the point (x, y) is selected by the occurrence of a crossing of a fixed level.

3.2 Slope distributions with asynchronous sampling in space

The asynchronous slope distribution of the space wave in the x- and y-directions at the fixed point (x_0, y_0) is the conditional distribution of the right hand side in (16) under the condition that $(X(\boldsymbol{s}), Y(\boldsymbol{s})) = (x_0, y_0)$. Now, there may be more than one solution and the condition has to be interpreted as an average over the possible solutions. For practical purposes, this is of minor importance, in cases when multiple solutions are rare. We use the technique used in [2] for the height distribution in the 2D Lagrange model.

The condition $\boldsymbol{\Sigma}(\boldsymbol{s}) = (X(\boldsymbol{s}), Y(\boldsymbol{s})) = (x_0, y_0)$ is a multiple crossing event, i.e. the level curves for the X- and Y-fields intersect each other. Such multiple crossing events can be analyzed by means of a generalized Rice formula for the number of marked crossings in multi-dimensional processes and fields. We will specifically use the results in [3, Thm. 6.4] on the expected number of marked roots of random equations.

In this context, the roots are the reference points with $\mathbf{\Sigma}(\boldsymbol{s}) = (x_0, y_0)$, and the marks are the slopes $\widetilde{\mathbf{L}}'(\boldsymbol{s}) = \mathbf{L}'(x_0, y_0)$ defined by (16). By stationarity, we can take $(x_0, y_0) = (0, 0)$, and define the number of unmarked and marked roots. Take the set $A = (-\infty, \ell_x] \times (-\infty, \ell_y] \subset \mathbb{R}^2$, and define

$$N_0 = \#\left\{\boldsymbol{s} \in \mathbb{R}^2; \mathbf{\Sigma}(\boldsymbol{s}) = (0,0)\right\},$$
$$N_0(A) = \#\left\{\boldsymbol{s} \in \mathbb{R}^2; \mathbf{\Sigma}(\boldsymbol{s}) = (0,0), \mathbf{L}'(\boldsymbol{s}) \in B\right\},$$

with subscript 0 standing for "asynchronous sampling at $(0,0)$".

Then $\mathsf{E}(N_0(A))/\mathsf{E}(N_0)$ is an approximation[1] to the bivariate distribution function of the asynchronous slopes at the origin, $\mathsf{P}(L_x \leq \ell_x, L_y \leq \ell_y)$.

To formulate the results, define the indicator function

$$I(\widetilde{\mathbf{L}}'(\boldsymbol{s}) \in A) = I\left\{\widetilde{L}_x(\boldsymbol{s}) \leq \ell_x, \widetilde{L}_y(\boldsymbol{s}) \leq \ell_y\right\}, \tag{17}$$

equal to one if the event occurs, and zero otherwise.

In the same way as the standard Rice formula includes the process derivative to take care of the "slope-biased sampling" at crossings, we have to introduce the derivative matrix,

$$\mathbf{\Sigma}'(\boldsymbol{s}) = \begin{pmatrix} X_u(\boldsymbol{s}) & Y_u(\boldsymbol{s}) \\ X_v(\boldsymbol{s}) & Y_v(\boldsymbol{s}) \end{pmatrix},$$

and its determinant, $\det \mathbf{\Sigma}'(\boldsymbol{s})$, to compensate for "area-bias". We formulate the theorem for $(x_0, y_0) = (0,0)$, without loss of generality, and denote by $p_{\mathbf{\Sigma}(\boldsymbol{s})}(0,0)$ the bivariate normal density of $(X(\boldsymbol{s}), Y(\boldsymbol{s}))$. The following theorem is a direct consequence of [3, Thm. 6.4].

Theorem 1. *(a) The expected number of solutions to $\mathbf{\Sigma}(\boldsymbol{s}) = (0,0)$ is given by*

$$\mathsf{E}(N_0) = \iint_{\mathbb{R}^2} \mathsf{E}\left(|\det \mathbf{\Sigma}'(\boldsymbol{s})| \mid \mathbf{\Sigma}(\boldsymbol{s}) = (0,0)\right) p_{\mathbf{\Sigma}(\boldsymbol{s})}(0,0,)\, \mathrm{d}\boldsymbol{s}. \tag{18}$$

(b) The expected number of solutions to $\mathbf{\Sigma}(\boldsymbol{s}) = (0,0)$ that satisfy $\widetilde{L}_x(\boldsymbol{s}) \leq \ell_x, \widetilde{L}_y(\boldsymbol{s}) \leq \ell_y$, is given by

$$\mathsf{E}(N_0(A)) = \iint_{\mathbb{R}^2} \mathsf{E}\left(|\det \mathbf{\Sigma}'(\boldsymbol{s})|\, I(\widetilde{\mathbf{L}}'(\boldsymbol{s}) \in A) \mid \mathbf{\Sigma}(\boldsymbol{s}) = (0,0)\right) p_{\mathbf{\Sigma}(\boldsymbol{s})}(0,0)\, \mathrm{d}\boldsymbol{s}. \tag{19}$$

[1] If only one root is possible, then the expression is exact. Otherwise, it is a weighted average of the distributions, taken over the reference points.

(c) The ratio $\mathsf{E}(N_0(A))/\mathsf{E}(N_0)$ *gives the observable distribution of slopes observed by asynchronous sampling over a large statistically homogeneous area. It is also equal to the observable slope distribution observed by asynchronous sampling in time at a fixed point.*

The expectations (18) and (19) are best found by Monte Carlo simulation of the six-dimensional Gaussian variable

$$\mathbf{R} = \mathbf{R}(\boldsymbol{s}) = \big(W_u(\boldsymbol{s}), W_v(\boldsymbol{s}), X_u(\boldsymbol{s}), X_v(\boldsymbol{s}), Y_u(\boldsymbol{s}), Y_v(\boldsymbol{s})\big),$$

given that $(X(\boldsymbol{s}), Y(\boldsymbol{s})) = (0, 0)$, followed by numerical integration over $\boldsymbol{s}$. In Section 5 we will present some examples of asynchronous slope distributions.

3.3 Space slope distribution at crossing points

For safety analysis of marine operations, the combined effect of wave height and wave slope may be more important than merely the slope distribution. In order to investigate how the asymmetry properties of the 3D Lagrange model depend on the wave height we derive the distribution when the slope is observed by synchronous sampling at the instances where $\mathbf{L}(x, y)$ has a crossing of a fixed level w_0, and in particular treat up- and downcrossings separately. Then, we also have to specify a direction along which the crossings are identified. Therefore, fix an axis (the x-axis), denote its direction $\theta = 0$, and define all directions relative to this direction.

We consider now crossings of the level w_0 by the process $\mathbf{L}(x, 0), x \in \mathbb{R}$. This means that we have to identify all reference points where $Y(\boldsymbol{s}) = 0$ and $W(\boldsymbol{s}) = w_0$, i.e. where two level curves in a bivariate Gaussian field intersect each other. In this context, the interesting roots are the reference points with

$$\mathbf{Z}(\boldsymbol{s}) := (W(\boldsymbol{s}), Y(\boldsymbol{s})) = (w_0, 0). \tag{20}$$

Each root corresponds to exactly one crossing of the level w_0 by the space wave along the x-axis, and we define the mark attached to a root as the ratio (16) at that crossing. The ratio between the expected number of marked and unmarked roots will give the observable distribution of the marks over all crossings.

We use a similar indicator function (17), as in the asynchronous case, but to take care of up- and downcrossings, separately, we modify it slightly, and define, for $\ell_x, \ell_y > 0$,

$$B^+ = (0, \ell_x] \times (-\infty, \ell_y],$$
$$B^- = [-\ell_x, 0) \times (-\infty, \ell_y].$$

The number of marked and unmarked up- and downcrossings of the level w_0 with reference point in a strip $[0, S] \times \mathbb{R}$ of finite width S, are denoted

$$N_S^{\pm} = \#\left\{\boldsymbol{s} \in [0,S] \times \mathbb{R}; \mathbf{Z}(\boldsymbol{s}) = (w_0, 0), \widetilde{L}_x(\boldsymbol{s}) \gtrless 0\right\},$$
$$N_S^{\pm}(B) = \#\left\{\boldsymbol{s} \in [0,S] \times \mathbb{R}; \mathbf{Z}(\boldsymbol{s}) = (w_0, 0), \widetilde{\mathbf{L}}'(\boldsymbol{s}) \in B^{\pm}\right\},$$

with $N_S = N_S^+ + N_S^-$, the total number of crossings. The "slope-biased sampling" at crossings is compensated by the derivative matrix

$$\mathbf{Z}'(\boldsymbol{s}) = \begin{pmatrix} W_u(\boldsymbol{s}) & Y_u(\boldsymbol{s}) \\ W_v(\boldsymbol{s}) & Y_v(\boldsymbol{s}) \end{pmatrix},$$

and its determinant, $\det \mathbf{Z}'(\boldsymbol{s})$. For a fixed pair $\boldsymbol{s} = (u, v)$, the slope (16) is just the ratio between two quadratic forms in a six-variate normal distribution, and its distribution can be found by integrating the multivariate density. However, we shall use the expression to find the *conditional* slope distribution of the space wave along the x-axis, which corresponds to conditioning on reference points $\boldsymbol{s} \in V_0$.

Theorem 2. *(a) The expected number of space wave up- and downcrossings of the level w_0, with reference point in a strip $[0, S] \times \mathbb{R}$ of width S, is*

$$\mathsf{E}(N_S^{\pm}) = S\,\mathsf{E}(N_1) = S \int_{v \in \mathbb{R}} \mathsf{E}(|\det \mathbf{Z}'(0,v)|\, I(\widetilde{L}_x(0,v) \gtrless 0) \\ \Big|\ \mathbf{Z}(0,v) = (w_0, 0))\, p_{\mathbf{Z}(0,v)}(w_0, 0)\, \mathrm{d}v, \quad (21)$$

where $p_{\mathbf{Z}(\boldsymbol{s})}(w, 0)$ is the bivariate normal density function of $\mathbf{Z}(\boldsymbol{s})$ at $(w, 0)$. (b) The expected number of up- and downcrossings of the level w_0 in the x-direction with reference points in $[0, S] \times \mathbb{R}$, and with slopes

$$|L_x(x, 0)| \le \ell_x, L_y(x, 0) \le \ell_y,$$

is given by

$$\mathsf{E}(N_S^{\pm}(B)) = S\,\mathsf{E}(N_1^{\pm}(B)) = S \int_{v \in \mathbb{R}} \mathsf{E}(|\det \mathbf{Z}'(0,v)|\, I(\widetilde{\mathbf{L}}'(\boldsymbol{s}) \in B_S^{\pm}) \\ \Big|\ \mathbf{Z}(0,v) = (w_0, 0))\, p_{\mathbf{Z}(0,v)}(w_0, 0)\, \mathrm{d}v. \quad (22)$$

(c) The ratio $\mathsf{E}(N_1(B^{\pm})/\mathsf{E}(N_1^{\pm})$ gives the long run (Palm) distribution of slopes at w_0-crossings by the space waves in the 3D Lagrange model. It is the limit, as $S \to \infty$, of the empirical distribution ratio $N_S(B^{\pm})/N_S^{\pm}$.

PROOF: Formula (22) is Theorem 6.4 in [3], with (21) as special case. (Note, that the fields are homogeneous, so the expectations are proportional to the strip width.) Part (c) is the limiting result for ergodic processes. □

The conditional expectations in (21) and (22) are most easily found by Monte Carlo simulation of the conditional six-dimensional Gaussian variable

$$\mathbf{R} = \mathbf{R}(\boldsymbol{s}) = \big(W_u(\boldsymbol{s}), W_v(\boldsymbol{s}), X_u(\boldsymbol{s}), X_v(\boldsymbol{s}), Y_u(\boldsymbol{s}), Y_v(\boldsymbol{s})\big),$$

given that $\mathbf{Z}(\boldsymbol{s}) = (w_0, 0)$, followed by numerical integration over v.

4 Slope distribution for time waves

4.1 The time wave and its geometry

4.1.1 The time wave

The Lagrange time wave, in a restricted sense, is the measured water height variation at a fixed point (x_0, y_0) in space as a function of time. With a more general view, one can also include the time variations of the geometric properties of the surface around the measuring point, in the time wave. Examples of such geometric properties are the gradient size and direction, and the wave front velocity and direction. In this section, we concentrate on the conditional properties of the surface observed at time instances when the water level at the measuring station crosses a fixed level.

To fix notation, we assume $(x_0, y_0) = (0, 0)$, and denote by

$$\boldsymbol{s_0}(t) = \boldsymbol{\Sigma}^{-1}(t, (0, 0))$$

the set of solutions to the equation $\boldsymbol{\Sigma}(t, \boldsymbol{s}) = (0, 0)$. For a fixed level w_0, a crossing by the time wave $t \mapsto L(t) := W(t, \boldsymbol{s}_0(t))$ occurs any time t for which there exists at least one reference point $\boldsymbol{s}$ where, simultaneously,

$$W(t, \boldsymbol{s}) = w_0, \quad \text{and} \quad \boldsymbol{\Sigma}(t, \boldsymbol{s}) = (0, 0). \tag{23}$$

Such triple crossings can be handled by [3, Thm. 6.4], on the expected number of joint crossings and the expected number of marked crossings. The mark can be any characteristic of the surface around the crossing. For future use we denote by $(t_k, \boldsymbol{s}_k)$, $k = 1, 2, \ldots$, the times and reference coordinates for the solutions (23) with $t_k > 0$.

Conditioned on a level crossing by the time wave, i.e. the occurrence of the event (23), one can be interested in the distribution of many different wave characteristics of practical importance. They can all be handled by the quoted theorem. In this paper we shall deal with time derivatives at

the times of crossings and of the surface gradients at these crossings. The physical interpretation of these quantities are the speed of increase and the steepness/direction of the wave front that hits the measuring station at the crossing.

4.1.2 Time derivative

The time wave, measured at location $(0,0)$, is equal to $W(t, \boldsymbol{s}_0(t))$, where

$$\begin{pmatrix} X(t, \boldsymbol{s}_0(t)) \\ Y(t, \boldsymbol{s}_0(t)) \end{pmatrix} = \begin{pmatrix} 0 \\ 0 \end{pmatrix},$$

whether or not there is one or many solution. Equations (12-13) give the time derivative at a crossing as

$$L_t(t) = W_t - \begin{pmatrix} W_u & W_v \end{pmatrix} \begin{pmatrix} X_u & X_v \\ Y_u & Y_v \end{pmatrix}^{-1} \begin{pmatrix} X_t \\ Y_t \end{pmatrix}.$$

If the inverse exists, the right hand expression is uniquely defined, and it gives the time wave derivative at each of the corresponding wave levels at $(0,0)$. As mentioned, for not so extreme cases, the probability of more than one solution is very low.

If the inverse in (15) does not exist, and

$$\det \begin{pmatrix} X_u & X_v \\ Y_u & Y_v \end{pmatrix} = 0,$$

then the measure point $(0,0)$ lies on a folding line, and the derivative can be left undefined.

4.2 Conditional distributions at time wave crossings

The conditional distributions of time slopes and space gradients in time waves can be formulated in an analogous way as the space wave quantities. With $(t_k, \boldsymbol{s}_k)$ equal to the times and reference coordinates for the occurred time wave crossings, define $N_T = \#\{t_k \in [0,T]\}$, as the number of unmarked time wave crossings, counted with multiplicity.

Time slopes and space gradients are examples of marks that are attached to the time wave crossings, and they are all defined in terms of the basic Lagrange processes

$$\mathbf{Z}(t, \boldsymbol{s}) = \big(W(t, \boldsymbol{s}), X(t, \boldsymbol{s}), Y(t, \boldsymbol{s})\big),$$

(extending the notation (20) from Section 3.3), and the derivatives

$$\mathbf{Z}'(t,\boldsymbol{s}) = \begin{pmatrix} W_t & X_t & Y_t \\ W_u & X_u & Y_u \\ W_v & X_v & Y_v \end{pmatrix}. \tag{24}$$

For any event A, defined for $Z'(t,\boldsymbol{s})$, write

$$N_T(A) = \#\left\{t_k \in [0,T]; \mathbf{Z}'(t_k,\boldsymbol{s}_k) \in A\right\},$$

the number of A-marked crossings. Obviously, by choosing an appropriate A-event, one can get any relative number of marked time wave crossings. We can then formulate the following theorem on the expected number of marked and unmarked time wave crossings; the proof is just a reference to [3, Thm. 6.4].

Theorem 3. *(a) The expected number of 3D Lagrange time wave crossings of the level w_0 in the time interval $[0,T]$, is*

$$\begin{aligned}\mathsf{E}(N_T) &= T\,\mathsf{E}(N_1)\\ &= T\int_{\boldsymbol{s}\in\mathbb{R}^2} \mathsf{E}(|\det \mathbf{Z}'(0,\boldsymbol{s})| \;\big|\; \mathbf{Z}(0,\boldsymbol{s}) = (w_0,\mathbf{0}))\, p_{\mathbf{Z}(0,0,v)}(w_0,\mathbf{0})\,\mathrm{d}\boldsymbol{s},\end{aligned}$$

where $p_{\mathbf{Z}(t,\boldsymbol{s})}(w,\mathbf{0})$ is the tri-variate normal density function of $\mathbf{Z}(t,\boldsymbol{s})$ at $(w,\mathbf{0})$.

(b) The expected number of marked crossings of the level w_0 in the time interval $[0,T]$, at which $\mathbf{Z}'(t_k,\boldsymbol{s}_k) \in A$, is, with $I(A)$ the indicator function for the event $\mathbf{Z}'(0,\boldsymbol{s}) \in A$,

$$\begin{aligned}\mathsf{E}(N_T(A)) &= T\,\mathsf{E}(N_1(A))\\ &= T\int_{\boldsymbol{s}\in\mathbb{R}^2} \mathsf{E}\left(|\det \mathbf{Z}'(0,\boldsymbol{s})|\, I(A) \;\big|\; \mathbf{Z}(0,\boldsymbol{s}) = (w_0,\mathbf{0})\right)\, p_{\mathbf{Z}(0,\boldsymbol{s})}(w_0,\mathbf{0})\,\mathrm{d}\boldsymbol{s}.\end{aligned}$$

(c) The ratio $\frac{\mathsf{E}(N_1(A))}{\mathsf{E}(N_1)}$ gives the long run (Palm) distribution of $\mathbf{Z}'(t_k,\boldsymbol{s}_k)$ observed at the w_0-crossings by the time wave in the 3D Lagrange model. It is the limit, as $T\to\infty$, of the empirical distribution ratio $\frac{N_T(A)}{N_T}$.

5 Examples

The purpose of this example is to show how the degree and direction of the spreading affects the front-back asymmetry of the Lagrange space waves with different degree of linkage in model (10). To clearly see the effects, we have chosen a moderate water depth, $h = 32\,\mathrm{m}$.

5.1 The model setup

5.1.1 The orbital spectrum

We will illustrate the theory on a model with Pierson-Moskowitz (PM) orbital frequency spectrum, i.e. the spectrum of the W-field, with un-directional, one-sided spectral density

$$S(\omega) = \frac{5H_s^2}{\omega_p(\omega/\omega_p)^5}\, e^{-\frac{5}{4}(\omega/\omega_p)^{-4}}, \quad 0 \le \omega \le \omega_c,$$

where $H_s = 4\sqrt{\mathsf{V}(W(t,u))}$ is the *significant wave height* in the W-process, and ω_p is the *peak frequency*, at which the spectral density has its maximum. The *peak period* is defined as $T_p = 2\pi/\omega_p$. We use fixed values, $H_s = 7\,\mathrm{m}$ and $T_p = 11\,\mathrm{s}$, for significant wave height and peak period, and assume a finite cut off frequency ω_c to obtain finite spectral moments and avoid small but high frequency wave components.

Note that H_s is defined as four times the standard deviation of the W-process, and that it is not exactly equal to the significant wave height in the resulting Lagrange wave process, since the two processes have different spectra and slightly different standard deviation; see [2] and Remark 4.

The average wave steepness is important for the degree of front-back asymmetry. For narrow-band spectrum it can be defined as the ratio, H_s/L_0, between the significant wave height and the peak wave length, $L_0 = 2\pi/\kappa_p$. In deep water, the steepness is equal to $\frac{2\pi H_s}{gT_p^2} \approx 0.037$, with the chosen H_s and T_p values. We will illustrate the distributions for waves at a finite water depth, $h = 32\,\mathrm{m}$, in which case the dispersion relation, (1), gives $L_0 \approx 160\,\mathrm{m}$ and approximate steepness 0.044. Both values are normal for high wind waves, cf. e.g., [12, Fig. 6.3] and [25, Fig. 2], even if the H_s-value is rather high for the chosen depth. The cut off frequency is $\omega_c = 2.5\,\mathrm{rad/s}$.

The unidirectional space waves, without spreading, were studied by Lindgren and Aberg [17], and the results from that paper will be used for comparison. Here, the directional spreading is taken as frequency independent and defined by the $\cos 2\theta$-function, so

$$S(\omega,\theta) = c(m)\, S(\omega) \cos^{2m}\left(\frac{\theta-\theta_0}{2}\right), \tag{25}$$

with different values for the spreading parameter m. An isotropic wave field corresponds to $m = 0$, while $m = \infty$ resembles unidirectional waves. We use $m = 0, 2, 5, 10, 20, 120,$ in this example. In the literature, values have been used between $m = 10$ for wind waves and up to $m = 75$ for old decayed swell; cf. [11], [21]. The six directional spectra are seen in Figure 5.

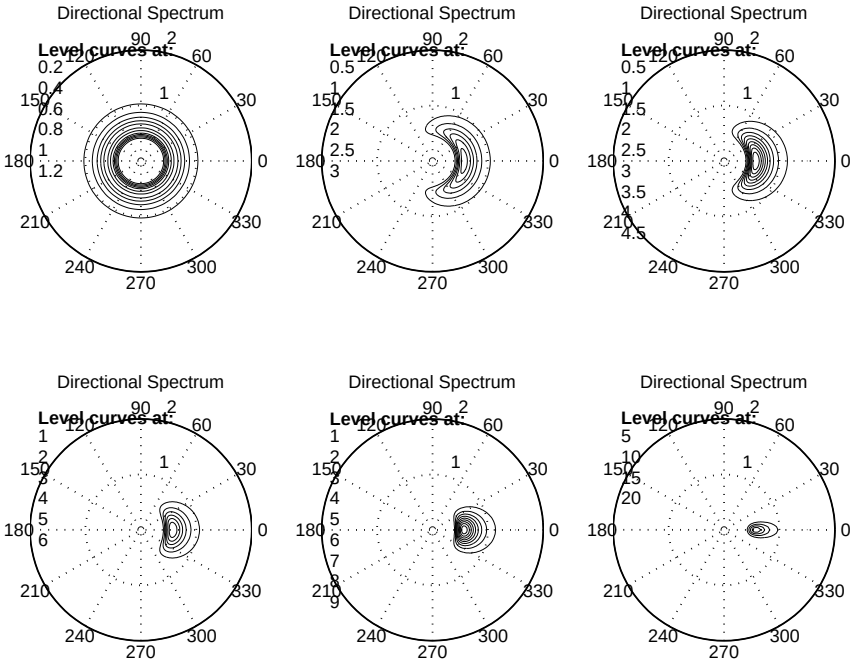

Figure 5: Directional Pierson-Moskowitz (PM) spectra for the $W(t, \boldsymbol{s})$-field, $S(\omega, \theta) = c(m)\, S(\omega) \cos^{2m}(2\theta)$; $m = 0, 2, 5, 10, 20, 120$, from top-left to bottom-right.

5.1.2 Summary measures of asymmetry and tail heaviness

To quantify the slope distributions with respect to up- and downcrossing asymmetry we will compute two measures based on quantiles. We consider upcrossing slopes and downcrossings slopes separately.

For asynchronous sampling, we denote, for $0 < q < 1$, by μ_q^+ and μ_q^- the q-quantiles in the subpopulation of positive and negative slopes, respectively. For synchronous sampling at up- and downcrossings, we define similarly, $\widetilde{\mu}_q^+$ and $\widetilde{\mu}_q^-$ as the q-quantiles in the upcrossing and downcrossings slopes, respectively, for a specified level.

We define the *slope asymmetry measure* for asynchronous slopes as

$$\lambda_q = -\mu_q^- / \mu_q^+,$$

for different values of q; see Figure 6. This measure was introduced with $q = 0.5$, as λ_{ST} in [16], giving the median.

As *measures of tail heaviness*, we will use the ratio between a large quantile and the median in the up- and downcrossing distributions; in the

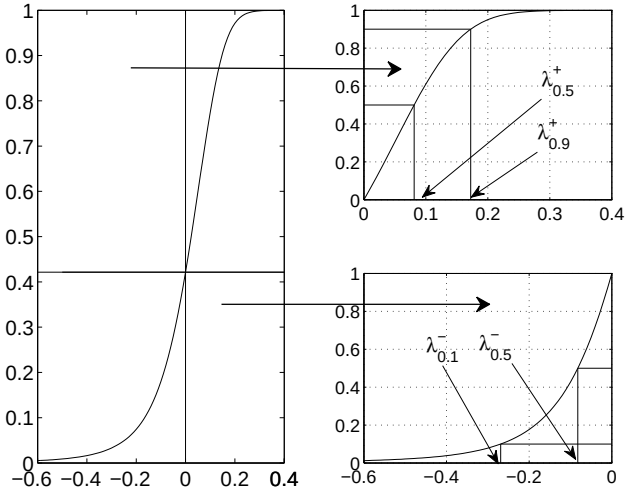

Figure 6: Quantile definitions $\mu^-_{0.1}, \mu^-_{0.5}, \mu^+_{0.5}, \mu^+_{0.9}$ defined for negative and positive asynchronous slope distribution. Left: CDF for all slopes; Right: CDF for positive (upper) and negative (lower) slopes.

asynchronous case, with $q > 0.5$,

$$\gamma^+_q = \mu^+_q/\mu^+_{0.5}, \qquad \gamma^-_q = \mu^-_q/\mu^-_{0.5}.$$

A larger γ-value indicates a heavier tail. To quantify the *asymmetry in tail behavior*, we will use for asynchronous sampling,

$$\delta_q = \gamma^-_q/\gamma^+_q.$$

For synchronous slope sampling at up- and downcrossings we define the corresponding quantities $\widetilde{\lambda}_q$, $\widetilde{\gamma}^\pm_q$, and $\widetilde{\delta}_q$, in the obvious way by replacing $\mu^\pm_q$ by the corresponding quantities $\widetilde{\mu}^\pm_q$.

The expectations of marked and unmarked crossings that lie behind the observable distributions in the theorems, are all found by Monte Carlo simulation of the conditional expectations, followed by numerical integration over the relevant spaces. Some details of the conditional distributions can be found in Appendix A.2. All simulations and computations are made in the MATLAB toolbox WAFO; see [26].

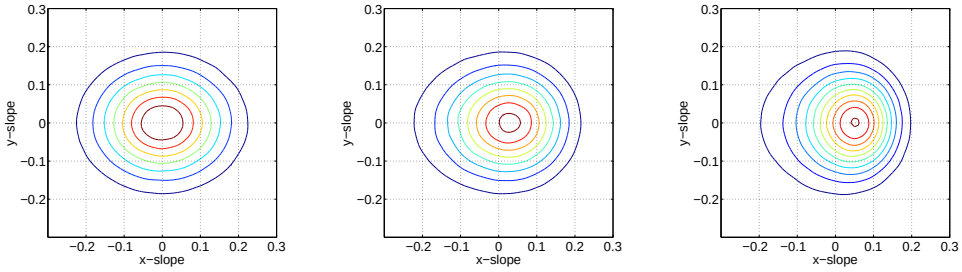

Figure 7: Asynchronous slope density functions in x- and y-direction. Orbital spectrum is PM with water depth $h = 32\,\mathrm{m}$. Directional spreading according to Figure 5 with $m = 20$. Linkage parameter in model (10) is $\alpha = 0, 0.8, 2.0$, from left to right.

5.2 Asynchronous sampling

The bivariate distribution function for slopes in x- and y-direction with asynchronous sampling in space is obtained, from Theorem 1, as

$$\begin{aligned} \mathsf{P}(L_x \le \ell_x, L_y \le \ell_y) &= \mathsf{E}(N_0(A(\ell_x, \ell_y)))/\mathsf{E}(N_0), \\ A(\ell_x, \ell_y) &= \{L_x(0,0) \le \ell_x, L_y(0,0) \le \ell_y\}. \end{aligned}$$

The expectations are found by Monte Carlo simulation of the conditional expectations in (18) and (19) followed by numerical integration over $\boldsymbol{s} \in \mathbb{R}^2$. The marginal distributions are obtained from the bivariate distribution by taking ℓ_x or ℓ_y equal to ∞. The probability densities are obtained by differentiation of the cumulative distribution functions, followed by moderate smoothing.

Figures 7 and 8 show densities of asynchronous slopes in x- and y-direction ("along-wind" and "cross-wind") for different degrees of linkage and spreading in model (10). Figure 7 shows the bivariate density for three selected combinations, while Figure 8 shows the marginal densities[2].

Table 1 contains the asymmetry and tail characteristic measures for along-wind slopes for two spreading models and for different degrees of linkage. The measures for the cross-wind direction are not shown in the table, since these distributions are symmetric and very close to normal as also can be seen in Figure 8.

The data in the table reveals some interesting features of the linked Lagrange model. The asymmetry between the positive and negative parts of the asynchronous slope distribution is only present for the more extreme

[2]Note that the densities in the right panel in Figure 1 are turned backwards to be compatible with the Cox and Munk figure.

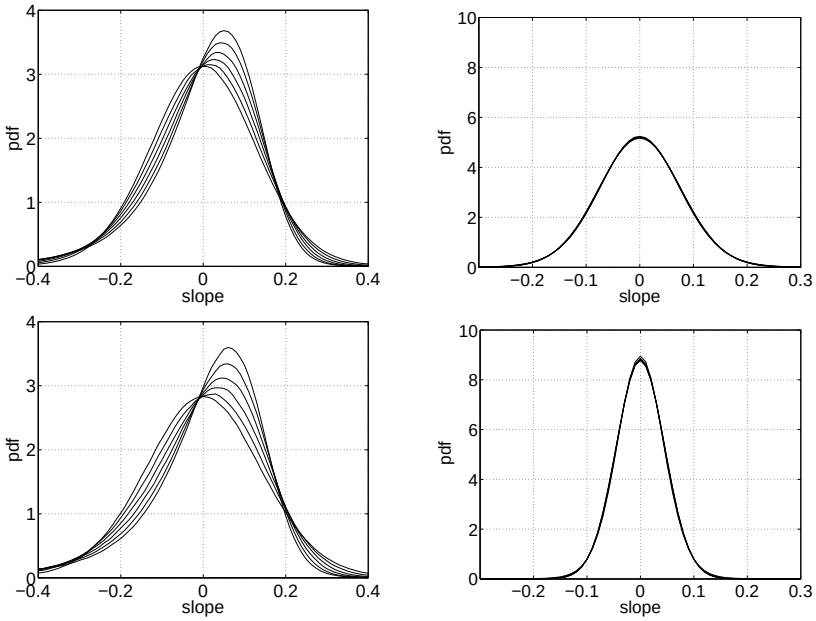

Figure 8: Asynchronous slope density functions in x- (left) and y-directions (right). Orbital spectrum is PM with water depth $h = 32$ m. Directional spreading according to Figure 5 with $m = 5$, (upper panels) and $m = 20$ (lower panels). Linkage parameters in model (10) are $\alpha = 0, 0.4, 0.8, 1.2, 1.6, 2.0$ (most skewed).

part of the two distributions. For slopes smaller than the median there is little asymmetry; this is verified from the complete data. For slopes larger in absolute value than the median in the two distributions, the asymmetry is large, however, as seen from the rapid increase with increasing linkage in the 90% quantile ratio $\lambda_{0.9}$.

For the tail behavior, the ratio $\gamma_{0.9}^-$ for negative slopes increases from near 2.44, which is the value for the normal distribution, to 3.27 with increased linkage, while the corresponding measure $\gamma_{0.9}^+$ for positive slopes decreases.

The effect of directional spreading is clear from the figure and from the table data. In the more concentrated spectrum, with $m = 20$, all the mentioned effects are more pronounced than for $m = 5$.

5.3 Slopes at up- and downcrossings

This example illustrates the synchronous sampling of slopes observed at up- and downcrossings of specified levels. The distribution function for slopes in the space waves, observed along the positive x-axis, i.e. in the

	$\alpha =$	0	0.4	0.8	1.2	1.6	2.0
$m = 5$	$\lambda_{0.5}$	1.00	1.01	1.02	1.02	1.02	1.01
	$\lambda_{0.9}$	1.00	1.10	1.21	1.33	1.45	1.56
	$\gamma^+_{0.9}$	2.48	2.38	2.29	2.22	2.17	2.13
	$\gamma^-_{0.9}$	2.48	2.60	2.74	2.90	3.09	3.27
	$\delta_{0.9}$	1.00	1.09	1.20	1.30	1.43	1.54
$m = 20$	$\lambda_{0.5}$	1.00	1.01	1.02	1.02	1.01	1.00
	$\lambda_{0.9}$	1.00	1.13	1.27	1.42	1.57	1.69
	$\gamma^+_{0.9}$	2.49	2.37	2.27	2.19	2.12	2.08
	$\gamma^-_{0.9}$	2.49	2.65	2.84	3.05	3.28	3.50
	$\delta_{0.9}$	1.00	1.12	1.25	1.39	1.54	1.68

Table 1: Skewness and excess measures in asynchronous sampling for waves with different degree of spreading and linkage.

main wave direction, is computed as in Theorem 2. The expectation ratio $\mathsf{E}(N_1(0,x])/\mathsf{E}(N_1(0,\infty))$ is obtained by Monte Carlo simulation of the conditional six-dimensional normal distribution, together with numerical integration over v in equations (21) and (22).

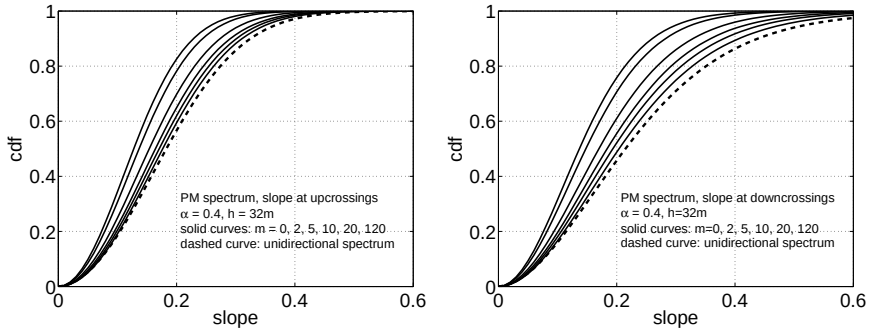

Figure 9: Cumulative distribution functions (CDF) for (absolute) space slopes at up- and downcrossings of the level $w_0 = \sigma = H_s/4$ along the main wave direction $\theta_0 = 0$. PM-spectra with different degree of spreading, from isotropic spectrum with $m = 0$ to almost unidirectional spectrum with $m = 120$, and unidirectional spectrum. The linkage parameter in model (10) is $\alpha = 0.4$.

Figure 9 shows the cumulative distribution functions for the (absolute values of the) slopes at upcrossings and downcrossings of the level $w_0 = \sigma = H_s/4$ for the six degrees of directional spreading in Figure 5. For comparison, the distribution for the unidirectional case is also plotted (dashed

curve). Obviously, the wave steepness decreases with increasing directional spreading, a fact that agrees with many other theoretical and empirical wave studies, as well as with the results for asynchronous sampling.

Also the front-back asymmetry decreases with increasing spreading, as can be expected. As a numerical measure of the asymmetry, we will use $\widetilde{\lambda}_q = -\widetilde{\mu}_q^-/\widetilde{\mu}_q^+$, where $\widetilde{\mu}_q^-$ and $\widetilde{\mu}_q^+$ are the q-quantiles in the downcrossing and upcrossing distribution functions, respectively, for a chosen level. Here we use $w_0 = H_s/4$. Table 2 shows the asymmetry measures, taken from the CDF:s in Figure 9. Note, how the asymmetry is more accentuated among the 10% steepest waves than among the average waves, with slopes near the median slope.

m	0	2	5	10	20	120	∞
$\widetilde{\lambda}_{0.5}$	1.07	1.08	1.10	1.12	1.13	1.16	1.18
$\widetilde{\lambda}_{0.9}$	1.14	1.16	1.20	1.23	1.27	1.31	1.35

Table 2: Front-back asymmetry measures $\widetilde{\lambda}_q = -\widetilde{\mu}_q^-/\widetilde{\mu}_q^+$, in synchronous sampling for PM-spectrum with different degree of spreading. Note that the asymmetry is more accentuated for the more extreme slopes.

As a final example, Figure 10 shows how the asymmetry depends on the mean wave direction in relation to the observation axis for the space waves. The spectrum is the directional PM-spectrum, (25), with $m = 10$, and main wave direction $\theta_0 = 0, \pi/4, \pi/2, 3\pi/4, \pi$. The linkage parameter in (10) is taken as $\alpha = 0.4$ as in Figure 9, and as $\alpha = 2$, for a more extreme case.

As see from the figure, the linkage has almost no effect on the up- or downcrossing slopes when the linkage (wind) is parallel to the wave crests, $\theta_0 = \pi/2$. The slopes at upcrossings are slightly smaller than at the downcrossings but the difference is small. Wind against the main wave direction gives steeper waves than wind along the wave direction, and the same holds for the intermediate cases, $\theta_0 = \pi/4$ and $\theta_0 = 3\pi/4$.

A Covariance structure

The stochastic space and time distributions in the 3D Lagrange model depend on the joint normal distribution of $W(t,\boldsymbol{s}), X(t,\boldsymbol{s}), Y(t,\boldsymbol{s})$ and their time and space derivatives, $Z'(t,\boldsymbol{s})$. The expressions for these covariances are derived from the transfer function for $X(t,\boldsymbol{s}), Y(t,\boldsymbol{s})$ from $W(t,\boldsymbol{s})$, according to (8).

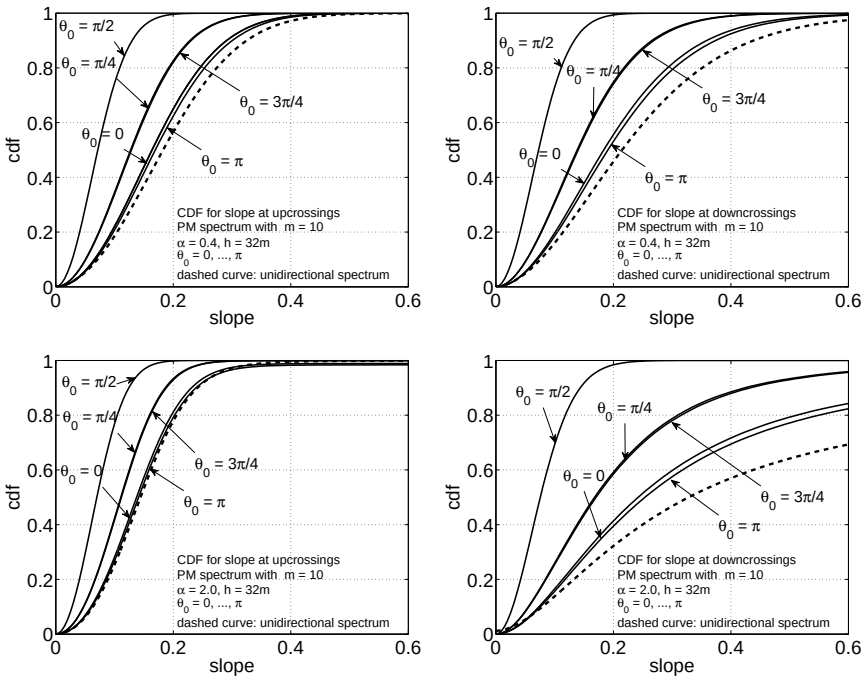

Figure 10: Mean wave directions influence on the cumulative distributions functions for (absolute) space slopes at up- (left) and downcrossings (right) along the x-direction of the level $w_0 = \sigma = H_s/4$. Spreading $m = 10$, and linkage parameter in model (10), upper diagrams: $\alpha = 0.4$, lower diagrams: $\alpha = 2.0$.

A.1 Covariances

For sake of reference, we list the explicit expressions of the covariances in terms of the directional spectrum $S(\theta, \omega)$ and the filter transfer function, expressed in terms of θ and ω as, (with $\kappa(\omega) = \|\boldsymbol{\kappa}(\omega)\|$),

$$\boldsymbol{H}(\theta, \omega) = \begin{pmatrix} \rho_x(\theta, \kappa(\omega))\, e^{i\psi_x(\theta,\kappa(\omega))} \\ \rho_y(\theta, \kappa(\omega))\, e^{i\psi_y(\theta,\kappa(\omega))} \end{pmatrix}.$$

The notation

$$r_{t0}^{wx}(t, \boldsymbol{\sigma}) = \mathsf{Cov}(W_t(0, \mathbf{0}), X(t, \boldsymbol{\sigma})) = \frac{\partial r^{w,x}(t, \boldsymbol{\sigma})}{\partial t},$$

etc., and $\boldsymbol{\kappa} = (\kappa_x, \kappa_y)$, $\boldsymbol{\sigma} = (u, v)$, is used for the different covariances. Integrations are over $\int_{\omega=0}^{\infty} \int_{\theta=-\pi}^{\pi}$, and we list only some selected combinations. The remaining combinations are obtained by obvious changes of u and v, or

of $X(t,\boldsymbol{\sigma})$ and $Y(t,\boldsymbol{\sigma})$. For short, we write

$$\begin{aligned}\gamma &= \gamma(\omega,\theta) = \boldsymbol{\kappa}\boldsymbol{\sigma} - \omega t,\\ \psi_k &= \psi_k(\omega,\theta) = \psi_k(\theta,\kappa(\omega)),\ \text{for } k = x,y,\\ \rho_k &= \rho_k(\omega,\theta) = \rho_k(\theta,\kappa(\omega)),\ \text{for } k = x,y.\end{aligned}$$

Covariances of $W(t,\boldsymbol{\sigma})$ and its derivatives:

$$\begin{aligned}r^{ww}(t,\boldsymbol{\sigma}) &= \iint \cos(\gamma)\, S(\omega,\theta)\,\mathrm{d}\omega\,\mathrm{d}\theta,\\ r^{ww}_{t0}(t,\boldsymbol{\sigma}) &= -r^{ww}_{0t}(t,\boldsymbol{\sigma}) = -\iint \omega\sin(\gamma)\, S(\omega,\theta)\,\mathrm{d}\omega\,\mathrm{d}\theta,\\ r^{ww}_{u0}(t,\boldsymbol{\sigma}) &= -r^{ww}_{0u}(t,\boldsymbol{\sigma}) = \iint \kappa_x\sin(\gamma)\, S(\omega)\,\mathrm{d}\omega\,\mathrm{d}\theta,\\ r^{ww}_{tu}(t,\boldsymbol{\sigma}) &= r^{ww}_{ut}(t,\boldsymbol{\sigma}) = -\iint \omega\kappa_x\cos(\gamma)\, S(\omega,\theta)\,\mathrm{d}\omega\,\mathrm{d}\theta,\\ r^{ww}_{tt}(t,\boldsymbol{\sigma}) &= \iint \omega^2\cos(\gamma)\, S(\omega,\theta)\,\mathrm{d}\omega\,\mathrm{d}\theta,\\ r^{ww}_{uv}(t,\boldsymbol{\sigma}) &= r^{ww}_{vu}(t,\boldsymbol{\sigma}) = \iint \kappa_x\kappa_y\cos(\gamma)\, S(\omega,\theta)\,\mathrm{d}\omega\,\mathrm{d}\theta.\end{aligned}$$

Covariances of $X(t,\boldsymbol{\sigma})$ and its derivatives:

$$\begin{aligned}r^{xx}(t,\boldsymbol{\sigma}) &= \iint \cos(\gamma)\,\rho_x^2\, S(\omega,\theta)\,\mathrm{d}\omega\,\mathrm{d}\theta,\\ r^{xx}_{t0}(t,\boldsymbol{\sigma}) &= -r^{xx}_{0t}(t,\boldsymbol{\sigma}) = -\iint \omega\sin(\gamma)\,\rho_x^2\, S(\omega,\theta)\,\mathrm{d}\omega\,\mathrm{d}\theta,\\ r^{xx}_{u0}(t,\boldsymbol{\sigma}) &= -r^{xx}_{0u}(t,\boldsymbol{\sigma}) = \iint \kappa_x\sin(\gamma)\,\rho_x^2\, S(\omega,\theta)\,\mathrm{d}\omega\,\mathrm{d}\theta,\\ r^{xx}_{tv}(t,\boldsymbol{\sigma}) &= r^{xx}_{vt}(t,\boldsymbol{\sigma}) = -\iint \omega\kappa_y\cos(\gamma)\,\rho_x^2\, S(\omega,\theta)\,\mathrm{d}\omega\,\mathrm{d}\theta,\\ r^{xx}_{tt}(t,\boldsymbol{\sigma}) &= \iint \omega^2\cos(\gamma)\,\rho_x^2\, S(\omega,\theta)\,\mathrm{d}\omega\,\mathrm{d}\theta,\\ r^{xx}_{uv}(t,\boldsymbol{\sigma}) &= r^{xx}_{vu}(t,\boldsymbol{\sigma}) = \iint \kappa_x\kappa_y\cos(\gamma)\,\rho_x^2\, S(\omega,\theta)\,\mathrm{d}\omega\,\mathrm{d}\theta.\end{aligned}$$

Cross-covariances of $W(t,\boldsymbol{\sigma})$ and $X(t,\boldsymbol{\sigma})$ and their derivatives:

$$\begin{aligned}r^{wx}(t,\boldsymbol{\sigma}) &= \iint \cos(\gamma+\psi_x)\,\rho_x\, S(\omega,\theta)\,\mathrm{d}\omega\,\mathrm{d}\theta,\\ r^{wx}_{t0}(t,\boldsymbol{\sigma}) &= -r^{wx}_{0t}(t,\boldsymbol{\sigma}) = -\iint \omega\sin(\gamma+\psi_x)\,\rho_x\, S(\omega,\theta)\,\mathrm{d}\omega\,\mathrm{d}\theta,\\ r^{wx}_{u0}(t,\boldsymbol{\sigma}) &= -r^{wx}_{0u}(t,\boldsymbol{\sigma}) = \iint \kappa_x\sin(\gamma+\psi_x)\,\rho_x\, S(\omega,\theta)\,\mathrm{d}\omega\,\mathrm{d}\theta,\end{aligned}$$

$$
\begin{aligned}
r_{tv}^{wx}(t,\boldsymbol{\sigma}) = r_{vt}^{wx}(t,\boldsymbol{\sigma}) &= -\iint \omega\kappa_y \cos(\gamma+\psi_x)\,\rho_x\,S(\omega,\theta)\,\mathrm{d}\omega\,\mathrm{d}\theta,\\
r_{tt}^{wx}(t,\boldsymbol{\sigma}) &= \iint \omega^2 \cos(\gamma+\psi_x)\,\rho_x\,S(\omega,\theta)\,\mathrm{d}\omega\,\mathrm{d}\theta,\\
r_{uv}^{wx}(t,\boldsymbol{\sigma}) = r_{vu}^{wx}(t,\boldsymbol{\sigma}) &= \iint \kappa_x\kappa_y \cos(\gamma+\psi_x)\,\rho_x\,S(\omega,\theta)\,\mathrm{d}\omega\,\mathrm{d}\theta.
\end{aligned}
$$

Cross-covariances of $X(t,\boldsymbol{\sigma})$ and $Y(t,\boldsymbol{\sigma})$ and their derivatives:

$$
\begin{aligned}
r^{xy}(t,\boldsymbol{\sigma}) &= \iint \cos(\gamma-\psi_x+\psi_y)\,\rho_x\,\rho_y\,S(\omega,\theta)\,\mathrm{d}\omega\,\mathrm{d}\theta,\\
r_{t0}^{xy}(t,\boldsymbol{\sigma}) = -r_{0t}^{xy}(t,\boldsymbol{\sigma}) &= -\iint \omega\sin(\gamma-\psi_x+\psi_y)\,\rho_x\,\rho_y\,S(\omega,\theta)\,\mathrm{d}\omega\,\mathrm{d}\theta,\\
r_{u0}^{xy}(t,\boldsymbol{\sigma}) = -r_{0u}^{xy}(t,\boldsymbol{\sigma}) &= \iint \kappa_x\sin(\gamma-\psi_x+\psi_y)\,\rho_x\,\rho_y\,S(\omega,\theta)\,\mathrm{d}\omega\,\mathrm{d}\theta,\\
r_{tv}^{xy}(t,\boldsymbol{\sigma}) = r_{vt}^{xy}(t,\boldsymbol{\sigma}) &= -\iint \omega\kappa_y\cos(\gamma-\psi_x+\psi_y)\,\rho_x\,\rho_y\,S(\omega,\theta)\,\mathrm{d}\omega\,\mathrm{d}\theta,\\
r_{tt}^{xy}(t,\boldsymbol{\sigma}) &= \iint \omega^2\cos(\gamma-\psi_x+\psi_y)\,\rho_x\,\rho_y\,S(\omega,\theta)\,\mathrm{d}\omega\,\mathrm{d}\theta,\\
r_{uv}^{xy}(t,\boldsymbol{\sigma}) = r_{vu}^{xy} &= \iint \kappa_x\kappa_y\cos(\gamma-\psi_x+\psi_y)\,\rho_x\,\rho_y\,S(\omega,\theta)\,\mathrm{d}\omega\,\mathrm{d}\theta.
\end{aligned}
$$

A.2 Joint distributions

The slope distributions in 3D Lagrange waves are expressed in Theorems 1-3 in terms of weighted integrals of conditional expectations of certain rational functions of the vertical and horizontal processes, and their partial space and time derivatives. Since the fields are jointly Gaussian, the multi-dimensional distribution is Gaussian, with a covariance matrix built by the covariances, $r_{tt}^{ww} = r_{tt}^{ww}(0,0) = \mathsf{V}(W_t(0,0))$, $r_{tu}^{wx} = r_{tu}^{wx}(0,0) = \mathsf{Cov}(W_t(0,0), X_u(0,0))$, etc. The expressions for the slope distributions are therefore mixed conditional averages of rational functions of conditional normal random variables, the weights given by a normal density.

A.2.1 Space wave

We present the explicit expressions for the space model in Theorem 2; the other distributions are simple variations of these expressions. We condition on

$$
\mathbf{Z}(\boldsymbol{s}) = (W(\boldsymbol{s}), Y(\boldsymbol{s}))^{\mathsf{T}},
$$

setting time to $t_0 = 0$, while the rational function includes the derivative determinant,

$$\det Z'(\boldsymbol{s}) = \det \begin{pmatrix} W_u(\boldsymbol{s}) & Y_u(\boldsymbol{s}) \\ W_v(\boldsymbol{s}) & Y_v(\boldsymbol{s}) \end{pmatrix},$$

and the slope, defined by (16),

$$L_x(\boldsymbol{s}) = \frac{Y_v(\boldsymbol{s})W_u(\boldsymbol{s}) - Y_u(\boldsymbol{s})W_v(\boldsymbol{s})}{Y_v(\boldsymbol{s})X_u(\boldsymbol{s}) - Y_u(\boldsymbol{s})X_v(\boldsymbol{s})}.$$

We separate the eight relevant variables into $\mathbf{Z} = \mathbf{Z}(\boldsymbol{s})$ and

$$\mathbf{R} = \big(W_u(\boldsymbol{s}), W_v(\boldsymbol{s}), X_u(\boldsymbol{s}), X_v(\boldsymbol{s}), Y_u(\boldsymbol{s}), Y_v(\boldsymbol{s})\big)^{\mathsf{T}}.$$

Then, the joint distribution of $(\mathbf{Z}^{\mathsf{T}}, \mathbf{R}^{\mathsf{T}})^{\mathsf{T}}$ is Gaussian with mean $\boldsymbol{\mu}$ and covariance matrix $\boldsymbol{\Sigma}$, partitioned as,

$$\boldsymbol{\mu} = \left(\begin{array}{cc|cccccc} 0 & v & 0 & 0 & 1 & 0 & 0 & 1 \end{array} \right)^{\mathsf{T}} = (\boldsymbol{\mu}_{\mathbf{Z}}^{\mathsf{T}} \mid \boldsymbol{\mu}_{\mathbf{R}}^{\mathsf{T}})^{\mathsf{T}},$$

$$\boldsymbol{\Sigma} = \left(\begin{array}{cc:cccccc} r^{ww} & r^{wy} & 0 & 0 & r^{wx}_{0u} & r^{wx}_{0v} & r^{wy}_{0u} & r^{wy}_{0v} \\ r^{yw} & r^{yy} & r^{yw}_{0\underline{u}} & r^{yw}_{0v} & r^{yx}_{0\underline{u}} & r^{yx}_{0\underline{v}} & r^{yy}_{0\underline{u}} & r^{yy}_{0\underline{v}} \\ \hdashline 0 & r^{wy}_{u0} & r^{ww}_{uu} & r^{ww}_{uv} & r^{wx}_{uu} & r^{wx}_{uv} & r^{wy}_{uu} & r^{wy}_{uv} \\ 0 & r^{wy}_{v0} & r^{ww}_{vu} & r^{ww}_{vv} & r^{wx}_{vu} & r^{wx}_{vv} & r^{wy}_{vu} & r^{wy}_{vv} \\ r^{xw}_{u0} & r^{xy}_{u0} & r^{xw}_{uu} & r^{xw}_{uv} & r^{xx}_{uu} & r^{xx}_{uv} & r^{xy}_{uu} & r^{xy}_{uv} \\ r^{xw}_{v0} & r^{xy}_{v0} & r^{xw}_{vu} & r^{xw}_{vv} & r^{xx}_{vu} & r^{xx}_{vv} & r^{xy}_{vu} & r^{xy}_{vv} \\ r^{yw}_{u0} & r^{yy}_{u0} & r^{yw}_{uu} & r^{yw}_{uv} & r^{yx}_{uu} & r^{yx}_{uv} & r^{yy}_{uu} & r^{yy}_{uv} \\ r^{yw}_{v0} & r^{yy}_{v0} & r^{yw}_{vu} & r^{yw}_{vv} & r^{yx}_{vu} & r^{yx}_{vv} & r^{yy}_{vu} & r^{yy}_{vv} \end{array} \right) = \left(\begin{array}{c:c} \boldsymbol{\Sigma}_{\mathbf{ZZ}} & \boldsymbol{\Sigma}_{\mathbf{ZR}} \\ \hdashline \boldsymbol{\Sigma}_{\mathbf{RZ}} & \boldsymbol{\Sigma}_{\mathbf{RR}} \end{array} \right).$$

The conditional distribution of $\mathbf{R}$, given that $\mathbf{Z} = (w_0, 0)^{\mathsf{T}}$, is Gaussian with mean $\boldsymbol{\mu}_{\mathbf{R}|\mathbf{Z}=(w_0,0)^{\mathsf{T}}}$ and covariance matrix $\boldsymbol{\Sigma}_{\mathbf{R}|\mathbf{Z}}$, given by,

$$\boldsymbol{\mu}_{\mathbf{R}|\mathbf{Z}=(w_0,0)^{\mathsf{T}}} = \boldsymbol{\mu}_{\mathbf{R}} + \boldsymbol{\Sigma}_{\mathbf{RZ}}\, \boldsymbol{\Sigma}_{\mathbf{ZZ}}^{-1} \begin{pmatrix} w_0 \\ -v \end{pmatrix} = \mathbf{A} + w_0\, \mathbf{B} + v\, \mathbf{C}, \quad \text{say,} \tag{26}$$

$$\boldsymbol{\Sigma}_{\mathbf{R}|\mathbf{Z}} = \boldsymbol{\Sigma}_{\mathbf{RR}} - \boldsymbol{\Sigma}_{\mathbf{RZ}}\, \boldsymbol{\Sigma}_{\mathbf{ZZ}}^{-1}\, \boldsymbol{\Sigma}_{\mathbf{ZR}}. \tag{27}$$

Consequently, the slope distribution in Theorem 2 is given in terms of weighted averages of a simple function in the six-dimensional normal distribution with these parameters.

A.2.2 Asynchronous sampling and crossings in time waves

For slope distribution with asynchronous sampling we have to use the conditional distribution of

$$R(\boldsymbol{s}) = (W_u(\boldsymbol{s}), W_v(\boldsymbol{s}), X_u(\boldsymbol{s}), X_v(\boldsymbol{s}), Y_u(\boldsymbol{s}), Y_v(\boldsymbol{s})),$$

given $(X(\boldsymbol{s}), Y(\boldsymbol{s})) = \mathbf{0}$, and for crossings in time waves, we have to use the conditional distribution of $\mathbf{Z}'(0, \boldsymbol{s})$ from (24), conditioned on the event $(W(0, \boldsymbol{s}), X(0, \boldsymbol{s}), Y(0, \boldsymbol{s})) = (w_0, \mathbf{0})$. The solutions have the same structure as for the space wave.

Acknowledgment

This work was carried out in the framework of the EU project SEAMOCS (contract MRTN CT 2005 019374). Two referees helped to clarify some important oceanographic details, for which we are grateful.

References

[1] Aberg, S. (2007a). Wave intensities and slopes in Lagrangian seas. *Adv. Appl. Prob.*, **39**, pp. 1020–1035.

[2] Aberg, S. and Lindgren, G. (2008). Height distribution of stochastic Lagrange ocean waves. *Probabilistic Engineering Mechanics*, **23**, pp. 359–363.

[3] Azaïs, J.M. and Wschebor, M. (2009) *Level sets and extrema of random processes and fields*. John Wiley & Sons, Hoboken.

[4] Bailey, R.J., Jones, I.S.F. and Toba, Y. (1991). The steepness and shape of wind waves. *J. Oceanographic Soc. Japan*, **47**, pp. 249–264.

[5] Bolin, D. and Lindgren, F. (2009). Spatial stochastic models generated by nested stochastic partial differential equations. *Preprints in Mathematical Sciences, 2009:14*. Lund University.

[6] Cox, C. and Munk, W. (1954). Measurement of the roughness of the sea surface from photographs of the sun's glitter. *J. Optical Soc. America*, **44**, pp. 838–850.

[7] Cox, C. and Munk, W. (1956). Slopes of the sea surface deduced from photographs of sun glitter. *Bull. Scripps Inst. Oceanogr.*, **6**, pp. 401–488.

[8] Ebuchi, N. and Kizu, S. (2002). Probability distribution of surface wave slope derived using sun glitter images from geostationary meteorological satellite and surface vector winds from scatterometers. *J. Oceanography*, **58**, pp. 477–486.

[9] Fouques, S., Krogstad, H.E. and Myrhaug, D. (2006). A second order Lagrangian model for irregular ocean waves. *Trans. of the ASME, J. Offshore Mechanics and Arctic Engineering*, **128**, pp. 177–183.

[10] Gjøsund, S.H. (2003). A Lagrangian model for irregular waves and wave kinematics. *Trans. of the ASME, J. Offshore Mechanics and Arctic Engineering*, **125**, pp. 94–102.

[11] Goda, Y. (1999). Numerical simulation of ocean waves for statistical analysis. *Marine Tech. Soc. J.*, **33**, pp. 5–14.

[12] Holthuijsen, L.H. (2007). *Waves in Oceanic and Coastal Waters*. Cambridge University Press.

[13] Kinsman, B. (1984). *Wind waves*, Dover Publications, New York.

[14] Lindgren, G. (2006). Slepian models for the stochastic shape of individual Lagrange sea waves. *Adv. Appl. Prob.* **38**, pp. 430–450.

[15] Lindgren, G. (2009). Exact asymmetric slope distributions in stochastic Gauss-Lagrange ocean waves. *Applied Ocean Research*, **31**, pp. 65–73.

[16] Lindgren, G. (2010). Slope distribution in front-back asymmetric stochastic Lagrange time waves. *Adv. Appl. Prob.*, **42**, pp. 489–508.

[17] Lindgren, G. and Aberg, S. (2008). First order stochastic Lagrange models for front-back asymmetric ocean waves. *J. Offshore Mechanics and Arctic Engineering*, **131** (2009) p. 031602-1 – 031602-8.

[18] Lindgren, G., Bolin, D. and Lindgren, F. (2010). Non-traditional stochastic models for ocean waves. *Eur. Phys. J. Special Topics*, **185**, pp. 209–224.

[19] Longuet-Higgins, M.S. (1982). On the skewness of sea-surface slopes. *J. Physical Oceanography*, **11** (1982) 1283–1291.

[20] Miche, M. (1944). Mouvements ondulatoires de la mer on profondeur constante ou décroissante. Forme limit de la houle lors de son déferlement. Application aux digues marines. *Ann. Ponts Chassées*, **114**, pp. 25–78.

[21] Mitsuyasu, H. et al. (1975). Observation of the directional spectrum of ocean waves using a cloverleaf buoy. *J. Physical Oceanography*, **5**, pp. 750–760.

[22] Plant, W.J. (2003). A new interpretation of sea-surface slope probability density functions. *J. Geophys. Res.*, **108(C9)**, 3295, doi:10.1029/2003JC001870.

[23] Podgórski, K. and Wegener, J. (2010). Non-Gaussian fields with vertical and horizontal asymmetries. *Preprints in Mathematics Sciences 2010:10*, Lund University, ISSN 1403-9338, pp. 1–54.

[24] Socquet-Juglard, H., Dysthe, K.B., Trulsen, K., Fouques, S., Liu, J. and Krogstad, H. (2004). Spatial extremes, shape of large waves, and Lagrangian models. In *Proc. Rogue Waves, Brest, 2004*. Available at http://www.ifremer.fr/web-com/stw2004/rw/fullpapers/krogstad.pdf.

[25] Tayfun, A. (2006). Distribution of wave steepness and surf parameter. *J. Waterw., Port, Coastal, Ocean Eng.*, **132(1)**, pp. 1–9.

[26] WAFO-group, (2011). *WAFO – a Matlab Toolbox for Analysis of Random Waves and Loads; Tutorial for WAFO Version 2.5*, Math. Stat., Centre for Math. Sci., Lund Univ., Lund, Sweden. URL http://www.maths.lth.se/matstat/wafo.

[27] Walsh, E.J., Banner, M.L., Wright, C.W., Vandemark, D.C., Chapron, B., Jensen, J. and Lee, S. (2008). The Southern Ocean waves experiment. Part III: Sea surface slope statistics and near-nadir remote sensing. *J. Physical Oceanography*, **38**, pp. 670–685.